N84-28928

QUANTUM CHEMICAL STUDY OF METHANE OXIDATION SPECIES

Status Report

Principal Investigator
Dr. Charles F. Jackels

Report for Period: December 4, 1983 - June 3, 1984

Institutional Address
Department of Chemistry
Wake Forest University
Winston-Salem, NC 27109

Cooperative Agreement No. NCC1-55

During the period of this report research was completed on the $^2A_1$ excited state and low-lying dissociative states of the methoxy radical. A manuscript was prepared that reports the characterization of the $^2A_1$ electronic state, the excitation energies and Franck-Condon factors for the $^2A_1$ - ^2E system, and the energies of intersection between the $^2A_1$ state and the nearby dissociative states. The minimum excitation energy needed for predissociation of methoxy is predicted along with the corresponding implications for atmospheric chemistry. This manuscript was submitted for publication to the Journal of Chemical Physics on August 1, 1984. A copy of this manuscript, titled "A potential-energy surface study of the $^2A_1$ and low-lying dissociative states of the methoxy radical", is attached to this report. It should be considered a complete and final report on the phase of the present research agreement that pertains to the methoxy radical.

Travel during this period of the agreement consisted of a trip by Dr. Jackels to NASA Langley Research Center in May, 1984. This trip was for the purpose of carrying on scientific discussions with Dr. D. H. Phillips of NASA pertaining to the funded research.

A potential-energy surface study of the $^2A_1$ and low-lying dissociative states of the methoxy radical

Charles F. Jackels

Department of Chemistry
Wake Forest University
Winston-Salem, North Carolina 27109

(Received

ABSTRACT

Low-lying bound and dissociative states of the methoxy radical have been studied at C_{3v} conformations using accurate ab initio quantum chemical techniques. A double-zeta quality basis set augmented with polarization and diffuse functions has been used throughout. The $\tilde{A}^2A_1$ excited state is found to have an equilibrium conformation with R_{CO}=1.614 Å, R_{CH}=1.091 Å, and θ_{HCO}=102.6°, and the three a_1 harmonic fequencies have been calculated (3239, 1308, and 733 cm^{-1}). The following excitation energies have been estimated: $\tilde{A}^2A_1 \leftarrow \tilde{X}^2E$ vertical excitation, 4.21 eV; $\tilde{A}^2A_1 \rightarrow \tilde{X}^2E$ vertical deexcitation, 3.52 eV; and the $\tilde{A}$ - $\tilde{X}$ system origin, 3.96 eV. The surface intersections of the $\tilde{A}^2A_1$ state with three low lying dissociative states ($^4A_2$, $^2A_2$, and ^4E) have been characterized. The threshold for predissociation has been estimated as 4.47 eV, corresponding to the $^2A_1$ - $^4A_2$ intersection. The rate of methoxy photolysis is estimated to be too small to warrant inclusion in atmospheric models.

PACS numbers: 31.20.Di, 33.80.Gj, 31.50.+w, and 94.10.Fa

I. INTRODUCTION

Alkoxy radicals form an important class of hydrocarbon oxidation intermediates in both combustion and atmospheric chemistry. Methane, which gives rise to the prototypic methoxy radical CH_3O, is introduced into the atmosphere in very large quantities by natural sources and is a global constituent of the troposphere. Although most of the methane is oxidized in the troposphere, enough of it reaches higher altitudes to give rise to stratospheric methane chemistry. Besides being important in the methane oxidation chemistry of both the upper[1] and lower[2] atmospheres, methoxy serves in a limited way as a model for more complicated alkoxy radicals. Being a highly reactive species, the CH_3O radical presents considerable experimental difficulties, but due to its relatively small size, it is well suited to accurate theoretical investigation. This paper reports the results of a quantum chemical study of the methoxy radical, with particular emphasis on its excited electronic states. A previous publication[3], hereafter referred to as I, reported a potential surface study that provided an overview of several electronic states of CH_3O and a detailed view of the ^2E ground state. The present paper reports results that place particular emphasis on the excited electronic states of the radical.

Methoxy is thought to be generated in the atmosphere by the reaction of the methylperoxy radical CH_3O_2 with reduced species such as NO, SO_2, or HO. Methylperoxy is formed by the reaction of CH_3 with O_2, the methyl radical being the product of hydrogen abstraction from methane by either the hydroxyl radical or oxygen atom. This chemistry is summarized by the following reactions:

$$CH_4 + OH \rightarrow CH_3 + H_2O \qquad (1)$$

$$CH_3 + O_2 \xrightarrow{M} CH_3O_2 \qquad (2)$$

$$CH_3O_2 + NO \rightarrow NO_2 + CH_3O \quad (3)$$

The major removal mechanism for atmospheric methoxy is thought to be its reaction with molecular oxygen to form HO_2 and formaldehyde,

$$CH_3O + O_2 \rightarrow HO_2 + CH_2O. \quad (4)$$

If the photolysis of CH_3O

$$CH_3O \xrightarrow{h\nu} CH_3 + O \quad (5)$$

were also to occur at a significant rate, it could be an important process because it would regenerate the methyl radical, with the subsequent formation of CH_3O_2 and further NO or SO_2 oxidation. This cyclical process would have the net effect of destroying O_2 and creating "odd oxygen" species such as NO_2 and O, which in principle could perturb the atmospheric ozone concentration. Consideration of Fig. 1, a reproduction of semiquantitative potential curves from paper I, suggests that the photolysis process of lowest energy would be excitaton to those vibrational levels of the $\tilde{A}^2A_1$ electronic state that would be predissociated by the intersecting repulsive states.

The methoxy radical has been studied by electronic absorption[4] and emission[5-7] spectroscopy, laser induced flourescence[8-10], laser magnetic resonance[11], ESR[12], and electron photodetachment spectroscopy.[13,14] In recent years, methoxy has been the subject of several theoretical investigations using various ab initio techniques.[3,15-19] These studies have included characterization of the ^2E ground and $^2A_1$ excited states, and have provided barrier estimates for isomerization and dissociation. The Jahn-Teller distortion of the ground state has been found[15,17c,19] to be small, with an energy decrease of only about 0.6 kcal/mole. The CH_3O spin-orbit coupling has also received theoretical attention.[17c,20]

In this paper are presented the results of a potential energy

surface study of the $\tilde{A}^2A_1$ excited state of the methoxy radical. The equilibrium geometry as well as a limited vibrational analysis of this excited state species is reported. Transition energies and Franck-Condon factors are predicted for both absorption and emission in the $^2A_1$ - ^2E system, which is responsible for the main features of the CH_3O visible-UV spectrum. Also, the low-lying repulsive states of methoxy, which were given a semiquantitative treatment in I, are accurately described in the regions of their intersections with the $^2A_1$ surface. These computed intersection energies provide an estimate of the minimum excitation energy required for predissociation. Using this estimate, the importance of Rxn. (5) in the atmosphere is evaluated.

During the course of the present study it was discovered that the computer program used to carry out the configuration interaction calculations of the ^2E ground state reported in paper I incorrectly omitted some double excitations from the master configuration list. This error was systematic in that it omitted the same configurations for each ^2E conformation but treated the $^2A_1$ state correctly. The effect of correcting this program error, when comparison is made with the results of paper I, is a uniform lowering of the extrapolated ^2E CI energies by approximately 0.010 hartree or 0.27 eV. This has a relatively small effect on the shape of the ^2E potential surface, but shifts that entire surface relative to the $^2A_1$ excited state, resulting in larger transition energies. The general conclusions of paper I are unaffected, but some of the numerical values reported have been revised. Accordingly, data tables in the present paper include both $^2A_1$ and corrected ^2E results. Since the changes are not of a qualitative nature, the discussions and analysis of paper I remain unchanged and are not reconsidered here.

II. GENERAL COMPUTATIONAL METHOD

The basis set and self-consistent field (SCF) method are the same as described in paper I. All computations were carried out at C_{3v} molecular conformations using a Cartesian Gaussian basis set of polarized double-zeta quality.[21-22] Equivalence restrictions were imposed on the e_x and e_y molecular orbitals, which constitutes a variational constraint for the ^2E ground state but not for the $^2A_1$ state. Relaxation of this constraint allows the ^2E SCF energy to decrease by about 1×10^{-3} hartrees; however, at the extrapolated CI level (see below) the decrease is less than 10^{-4} hartrees.

A different set of computer programs[23] was used for the present configuration interaction (CI) studies than for those reported in paper I. However, the methods are essentially the same. The details of the CI calculations will be discussed in the appropriate sections that follow, with only a general description given here. The A_k perturbation theory technique of Gershgorn and Shavitt[24] was used to select the most important configurations for inclusion in the wave functions. The selection procedure accepted or rejected a particular space configuration, with its entire set of spin couplings, based upon the sum of the A_k contributions for that set. The configurations were first ordered by their estimated energy contributions. Then, beginning with the least important one, configurations were rejected in sequence until the sum of the energy contributions for the rejected configurations was equal to τ, the cumulative selection threshold.[25] This method is designed to neglect a constant amount of correlation energy, and therefore is expected to yield balanced treatments of the various electronic states and the different regions of their potential energy surfaces.

There were two types of master configuration lists used in this work. In the type of calculation known as "all singles and doubles", the selection procedure was based upon a master list containing all single and double excitations from the root set configurations. In some of the potential surface calculations a "first-order" master list[26], containing those single and double excitations (with respect to the root set) with no more than one electron outside the valence space, was generated and subjected to the cumulative threshold selection procedure. This treatment is expected to yield balanced results when applied to the same state at similar conformations, thus generating potential surfaces which are displaced from, but nearly parallel to, more accurately determined ones. It is not expected that the "first-order" approach will result in such a well balanced treatment for different electronic states. Consequently, in this study energy differences between states were computed using the "all singles and doubles" configuration list.

To obtain improved CI convergence and to define meaningful valence space orbitals for the first-order calculations, approximate natural orbitals (ANO's) were used throughout. At each conformation the ANO's were obtained from preliminary CI calculations using several hundred of the most important configurations. After freezing[27] those orbitals that were occupied in the root set configurations, the ANO's were obtained as the natural orbitals[28] of these small CI expansions. Throughout this work, the oxygen and carbon 1s core orbitals remained fully occupied, and the corresponding core correlation ANO's (zero occupancy) were discarded.

III. FIRST-ORDER POTENTIAL ENERGY SURFACES

A. Method.

At each conformation the SCF wave functions and ANO's were obtained for both states by the procedures described in Section II above and in paper I. The CI root sets consisted of the dominant configuration for each state

$$\ldots(3a_1)^2(4a_1)^2(5a_1)^2(1e)^4(2e)^3 \qquad (^2E) \qquad (6)$$

$$\ldots(3a_1)^2(4a_1)^2(5a_1)^1(1e)^4(2e)^4 \qquad (^2A_1) \qquad (7)$$

Although in paper I a multiconfiguration root set was used for the ^2E state, only the dominant term is needed for the present range of important molecular conformations. The $^2A_1$ and ^2E first-order master lists contained, respectively, 12 159 and 8800 spin couplings (CSF's). Using a cumulative threshold of $\tau=2.5 \times 10^{-3}$ hartree, final configuration lists contained approximately 4500($^2A_1$) and 3400(^2E) CSF's at each conformation. Typically, these truncated configuration lists accounted for 98-99% of the estimated (A_K) first-order correlation energy, and the most important rejected configurations had estimated contributions of approximately 7×10^{-6} hartree.

B. Results and discussion

1. ^2E and $^2A_1$ equilibrium geometries

The C_{3v} conformations corresponding to the minimum first-order CI energies are given in Table I for the ^2E and $^2A_1$ states of methoxy. For comparison, three other recent ab initio results for the ground state are given, and the agreement is reasonable. There is one previous theoretical result[15] for the $^2A_1$ state, which utilized a smaller basis set (DZ) in an SCF study. Taking into account the differences in method, these results are also in reasonable agreement. In paper I a more detailed comparison was made of the same studies for

the methoxy ground state. The $^2A_1 \leftarrow {}^2E$ transition can be viewed as the excitation of an electron from the C-O σ-bonding orbital ($5a_1$) into the nonbonding π-orbital on oxygen (2e). In the excited state, the C-O bond is formally a one electron bond and the bond length is much longer than in the ground state. The C-H bond lengths are shortened a small amount by the excitation, and the HCO bond angle is decreased by 6-7°. This is consistent with a picture of the $-CH_3$ moiety gradually assuming the planar (D_{3h}) geometry of the free methyl radical[29] (R_{CH}=1.075 Å) as the C—O distance is increased.

2. Harmonic vibrational energies

The first-order potential surfaces were least-squares fitted to polynomials in the variables

$$\begin{aligned} \Delta R_{CO} &= R_{CO} - R^e_{CO}, \\ \Delta R_{CH} &= R_{CH} - R^e_{CH}, \\ \Delta\theta_{HCO} &= \theta_{HCO} - \theta^e_{HCO}, \end{aligned} \tag{8}$$

where the superscript "e" denotes the value of the coordinate at the minimum of the potential function. The general form of the polynomial is given by

$$E = E_0 + k_{200}(\Delta R_{CO})^2 + k_{110}\Delta R_{CO}\Delta R_{CH} + k_{020}(\Delta R_{CH})^2 + k_{101}\Delta R_{CO}\Delta\theta_{HCO} + k_{011}\Delta R_{CH}\Delta\theta_{HCO} + k_{002}(\Delta\theta_{HCO})^2 + \ldots, \tag{9}$$

where bond lengths are in bohrs, angles in degrees, and the energy in hartrees. The full ^2E and $^2A_1$ data sets contained, respectively, 86 and 99 points, which were distributed nonuniformly around the equilibrium geometry within the ranges: $R^e_{CO} \pm 0.2$ a_o, $R^e_{CH} \pm 0.1$ a_o, and $\theta^e_{HCO} \pm 13°$. Quadratic and cubic fits were made to these data sets as well as to subsets in which the points furthest from the equilibrium geometries had been deleted. The smaller sets contained 59 ^2E and 76 $^2A_1$ data points. Although the various data fits were fairly similar,

the force constants obtained from the cubic fits to the smaller data sets yielded the most accurate vibrational frequencies where comparison with experiment could be made. The quadratic force constants obtained from these cubic functions are presented in Table II.

The values of the force constant k_{200} for the two electronic states are consistent with the C-O bond being much weaker in the $^2A_1$ state than in the ground state. There is considerable variation (20%) in the value of this force constant as obtained from the various analytical fits. Since k_{200} has a dominant effect on the calculated C-O stretching frequency, attempts were made to reduce the uncertainty in this force constant by using more flexible potential functions. A full quartic fit to the 99-point $^2A_1$ data set was attempted, but the statistical uncertainties in the resulting force constants were unacceptably large. To see if a partial quartic fit would be an improvement, the cubic polynomial was supplemented by the fourth order term in ΔR_{CO}. Inclusion of this term had little effect on k_{200}, and the fit was unsatisfactory because of numerical difficulties in locating the minimum of the potential function. It was concluded that the $^2A_1$ data set was not complete enough to yield meaningful quartic constants. The difficulties involved in selecting an adequate grid of points for the purpose of obtaining well-defined higher force constants have been discussed by others.[30]

The Wilson FG formalism[31-32] was used with the force constants in Table II to obtain the harmonic vibrational frequencies and normal modes of a_1 symmetry for the CH_3O and CD_3O radicals. These frequencies are presented in Table III. For both electronic states, the agreement with experimental results is reasonably good. The theoretical results of Saebo et al.[19] were obtained at the Hartree-Fock level and,

according to those authors, should be reduced by 10% before comparison with experiment. After this scaling, these theoretical results are also consistent with the present ones. Analysis[32] of the normal-coordinates in terms of the internal coordinates gives the following dominant contributions: ν_1 - symmetric C-H stretch; ν_2 - symmetric HCO bend (umbrella mode); and ν_3 - CO stretch. For most of the entries in Table III the internal coordinates are almost entirely unmixed, and the above identifications represent nearly all of the normal mode character. However, in the $^2A_1$ state of both isotopic species the ν_3 mode has 18-20% bending character, with the HCO angle decreasing slightly as R_{CO} increases. Also, in the ^2E state of CD_3O the CO stretch and DCO bend are mixed strongly, giving 30% CO stretch character to ν_2 and 40% bend character to ν_3. This strong mixing in CD_3O and its implications for spectral assignments were discussed in paper I.

3. Anharmonic vibrational energies.

For comparison with the methoxy spectra, which involve long progressions in the C-O stretch, it is necessary to include anharmonic contributions in the theoretical estimates of the higher vibrational levels. Two one-dimensional vibrational models were used, both of which treated methoxy as a pseudo diatomic molecule. In the first approach, the HCO bond angles and H-C bond lengths were frozen at their equilibrium values, and the C-O distance was chosen as the vibrational coordinate. The potential curve for this model was defined as the cut through the methoxy surface that is generated by varying the (CH_3)-O distance with the other coordinates fixed. The second approach was similar, except that the cut through the potential surface was taken along the direction of the ν_3 normal coordinate. This coordinate,

which in general combines motion along all three internal coordinates, is mass weighted, and the pseudo diatomic is treated as a one dimensional oscillator with a reduced mass of unity. The finite difference method described by Tobin and Hinze[33] was used to numerically integrate the resulting one-dimensional vibrational Schroedinger equations.

The potential curves for both models were generated from the cubic fits to the larger data sets (86 and 99 points). To get a well behaved surface at intermediate values of R_{CO}, it was found necessary to extend the $^2A_1$ data set by including points with ΔR_{CO} values as large as 1.0 a_o. Since the cubic potential function, Eq.(9), is designed to describe the potential surface near the equilibrium geometry, the cuts through this surface were smoothly extended with Morse-type functions to larger and smaller values of the vibrational coordinates. In Fig. 2 are presented the two resulting potential curves for the $^2A_1$ state. They are plotted on the same scale by using mass weighted coordinates that in each case would correspond to an oscillator of unit mass. For equal values of the mass weighted coordinates, the R_{CO} values for the two curves differ slightly as indicated in the figure caption.

The computed vibrational energy levels, presented in Table IV, show that the two anharmonic models differ very little for the ^2E state, because in this case the ν_3 normal coordinate is almost pure C-O stretch. However, the difference between the two sets of levels is much larger for the $^2A_1$ state where the ν_3 normal coordinate includes considerable HCO bending character. The normal coordinate potential curve is seen in Fig. 2 to rise somewhat less steeply with increasing R_{CO} than does the "C-O distance" curve, resulting in more closely spaced vibrational levels. In the vicinity of the sixth or seventh

vibrational level the differences between the two sets of results are nearly as large as the intervals between levels. From the electronic absorption spectrum (Table I of Ref.4), the separation of the v'=6 and v'=0 levels of the $^2A_1$ state is calculated to be 3847 cm^{-1}. As shown in Table IV of the present work, the same separation is calculated to be 4286 cm^{-1} using the C-O distance as vibrational coordinate and 3904 cm^{-1} using the ν_3 normal coordinate. This comparison favors use of the normal coordinate to describe the lower lying vibrational levels. A similar comparison for the ^2E state also favors the normal coordinate approach but is less compelling, because in that case the two models are not very different.

IV. ACCURATE TRANSITION ENERGIES FOR THE $\tilde{A}^2A_1$ - $\tilde{X}^2E$ SYSTEM

A. Method.

The procedures used in this part of the study were designed to provide well-balanced treatments of the methoxy A and X electronic states so that accurate transition energies could be calculated. SCF calculations were carried out for each state [Eqs. (6)-(7)] and the corresponding ANO's were obtained. Master lists containings 41 740 ^2E and 41 047 $^2A_1$ spin configurtions were generated by including all single and double excitations with respect to the appropriate root (SCF) configuration. All single excitations were retained, and the double excitations were subjected to the A_k selection procedure using a cumulative threshold τ. CI energies $E(\tau)$ were obtained at three values of τ, fit to a straight line, and extrapolated[34] to zero threshold. The smallest threshold used in each case corresponded to inclusion of approximately 10 000 spin configurations.

To account in an approximate manner for the most important effects of quadruple excitations, Davidson's[35] correction formula was used,

$$\Delta E_q = (1 - C_0^2)\Delta E_d, \qquad (10)$$

where ΔE_d is the correlation energy due to the entire set of double excitations, ΔE_q is the analogous quantitiy due to quadruple excitations, and C_0 is the coefficient of Φ_{SCF} in the "all doubles" CI. In this work, the quantity ΔE_d was estimated to be equal to the extrapolated "singles plus doubles" correlation energy, and C_0 was taken from the CI calculation at the smallest of the selection thresholds.

The transition energies have been corrected for the vibrational zero point energy. All of the degenerate (e-type) vibrational frequencies have been recently calculated[19] for the ^2E state, but a

complete $^2A_1$ set is not available. Therefore, we have neglected the zero point contributions of the e-type modes, which is equivalent to assuming that they are the same in both states and cancel. For the a_1 modes the vibrational corrections are explicitly obtained from the values reported in Table III.

B. Results and discussion.

1. $\tilde{A}^2A_1 \leftarrow \tilde{X}^2E$ vertical excitation energy.

The vertical excitation energy is taken as the difference between the $\tilde{A}$ and $\tilde{X}$ state energies as computed at the ground state equilibrium geometry (Table I). For both states, the cumulative selection thresholds used in the extrapolated CI calculations were 40, 25, and 15×10^{-3} hartree. In Table V are listed the total energies obtained at the various stages of the calculation, and Table VI presents the transition energies obtained at these different levels. Inclusion of the correlation energy via CI makes a significant contribution to each of the three transition energies. This is to be expected, because the C-O bonding is qualitatively different in the two states. The vertical excitation energy is affected very little by either the extrapolation procedure or the correction for quadruple excitations. The vibrational correction is small but significant and is calculated by including the zero point energies of ν_{1-3} for the ^2E state and ν_{1-2} for the $^2A_1$ state (see Table III). This assumes that only the one normal mode (ν_3) is excited in absorption, which is consistent with the experimental spectrum. The "best" vertical excitation energy from this work, 4.21 eV, agrees very well with the position of the intensity maximum of the absorption spectrum[4], which appears to be one of the vibrational bands assigned as $v'=4$ or 5 (4.23 or 4.31 eV). This value also agrees very well with the position of the most intense band of the fluorescence

excitation spectrum, 4.23 eV.[10b]

As a further comparison with experiment, Franck-Condon factors were calculated for the $\tilde{A}^2A_1(v') \leftarrow \tilde{X}^2E(v''=0)$ progression using the anharmonic vibrational model with the C-O distance as the vibrational coordinate. It would be preferable to use the vibrational treatments based upon the ν_3 normal coordinates. However, because these coordinates are not the same for the two electronic states, a simple one dimensional integration of the vibrational overlap is not appropriate. Using the coordinate R_{CO}, the Franck-Condon factors as relative per centages for v'=0-9 are: 10, 38, 74, 97, 100, 84, 61, 39, 22, and 11. The largest of these values is at v'=4, which agrees reasonably well with the assigned band of maximum intensity (Fig. 1 of Ref. 4). However, the Franck-Condon factors calculated for v' greater than 4 appear to be somewhat smaller than those reported in Ref. 4. It is difficult to make a detailed comparison with the experimental intensities because the profile of the spectrum seems to suggest the presence of some additional underlying structure at the shorter wave lengths.

2. $\tilde{A}^2A_1 \rightarrow \tilde{X}^2E$ vertical deexcitation energy.

The vertical transition energy was also calculated at the equilibrium geometry of the $^2A_1$ excited state (Table I), and the results are given in Tables V-VI. The CI extrapolations used the same thresholds given in the previous section. In this case the inclusion of electron correlation causes an increase in the transition energy that is about twice as large as for vertical excitation. This is mostly because correlation of the C-O sigma bonding electrons in the ^2E state becomes increasingly important at larger C-O distances. This is reflected by the fact that in the ^2E wave function the coefficient of

the $\sigma^2 \rightarrow \sigma^{*2}$ excitation

$$...(3a_1)^2(4a_1)^2(6a_1)^2(1e)^4(2e)^3, \qquad (11)$$

increases from about 0.06 at the ground state equilibrium geometry to about 0.09 at that of the excited state. The vibrational correction was calculated by including the zero point energies of ν_{1-3} for the $^2A_1$ state and of ν_{1-2} for the ^2E state (Table III).

The calculated transition energy of 3.52 eV can be compared with the intensity of emission bands originating in the $\tilde{A}^2A_1$ (v'=0) state. The work of Inoue et al.[10b] gives the maximum emission intensity at the v"=3 band with an energy of 3.53 eV. The results of Sutoh et al.[6] are also in excellent agreement with the present calculations. For the $\tilde{A}^2A_1(v'=0) \rightarrow \tilde{X}^2E(v")$ progression in emission the Franck-Condon factors were also calculated, and the relative per cent values obtained for v"=0-8 levels are: 8, 35, 74, 100, 97, 70, 38, 15, and 4. The experimental data for this emission (Fig. 7 of Ref. 10b) is in relatively good agreement with these values.

3. The $\tilde{A}$-$\tilde{X}$ system origin.

The energy of the (0-0) band of methoxy is obtained by comparing the calculations for the two states at their respective equilibrium geometries. The vibrational correction is obtained by including all three a_1 modes ν_{1-3} of each state. The result, as given in Table VI, is a calculated system origin of 3.96 eV. This number is to be compared with the most recent experimental assignment of the origin in both absorption[4] and emission[10b] to the band at 3.91 eV. This level of agreement is consistent with the quality of the theoretical results, with the almost exact agreement noted in the previous section being somewhat fortuitous. There has been some difficulty in determining the system origin of methoxy, with earlier reports[5a,7,10a] assigning it to

spectral features at 3.78 and 4.07 eV. It is expected that the present theoretical procedures should estimate the transition energies with an uncertainty of 0.05-0.1 eV, placing the assignment of 4.07 eV slightly outside of the error bounds and the one at 3.78 clearly beyond them. The present results confirm the most recent experimental assignment (3.91 eV) as being correct.

4. Use of two-configuration ^2E reference state.

As noted above, the configuration that introduces left-right correlation of the C-O σ-bonding electron pair [Eq. (11)], becomes increasingly important in the ^2E wave function at larger C-O distances. At dissociation this configuration should be included in an MCSCF treatment and in the CI root set in order to obtain a qualitatively correct description of the wave function. Since the C-O distance is quite large at the A state equilibrium geometry, the adequacy of the single configuration approach to the present problem was assessed by repeating the ^2E calculations with Conf. (11) included in the MCSCF wave function and in the CI root set. The $^2A_1$ state does not require a comparable multiconfiguration treatment because Conf. (7) strongly dominates the wave function at the molecular conformations being considered. Because the C-O bond in the $^2A_1$ state is formally a one-electron bond, the single configuration treatment gives qualitatively correct dissociation to the neutral methyl and oxygen atom species. Additional root set configurations are only required at C-O distances of at least 5 a_o in order to correctly describe the electronic state of the oxygen atom.

The ^2E calculations with Confs. (6) and (11) in both the MCSCF wave function and the CI root set yielded extrapolated CI energies approximately $3\text{-}6\times10^{-3}$ h lower than did the single configuration

calculations. However, because some of the most important quadruple excitations, those that are doubly excited with respect to configuration (11), are explicitly included in the wave function, the Davidson correction ΔE_q becomes smaller in this multiconfiguration case. The net result of these two opposite effects is that the calculated system origin and vertical excitation energy would be decreased by 0.01 eV, and the vertical deexcitation energy would be increased by 0.04 eV. These changes would have no significant impact on the previous discussions.

5. Analysis of the $^2A_1$ wave function.

A detailed analysis of both the ^2E and $^2A_1$ wave functions at the ground state equilibrium geometry was presented in paper I. The present work does not require any elaboration on that discussion but makes possible an analysis of the $^2A_1$ wave function at its equilibrium conformation. The wave function is very similar to the one previously discussed in I. Since the C-O bond length is much longer at the $^2A_1$ equilibrium geometry than at that of the ground state, one might expect that the charge distribution would begin to rearrange in a way that would resemble dissociation. In particular, the $5a_1$ molecular orbital, which is the C-O σ-bonding orbital at short C-O distances, becomes the non-bonding p-orbital on carbon at dissociation. However, at the $^2A_1$ equilibrium geometry the $5a_1$ orbital, Fig. 3, has not begun to localize on carbon but is still very much a bonding orbital with the largest part of its density on oxygen. Based upon the most complete $^2A_1$ CI wave function used in this study, there is a charge transfer of about 0.5 electron from the hydrogen atoms to oxygen, with the carbon atom being essentially neutral. The electric dipole moment is calculated to be 3.8 Debye.

V. SURFACE CROSSINGS AND PREDISSOCIATION

A. Experimental background.

The well-studied hydroxyl radical has an electronic structure similar to that of methoxy. The $\tilde{A}$ state of OH shows evidence of strong predissociation at the v'=5 vibrational level, with weaker predissociation extending to the higher rotational levels of the v'=0 state.[36-38] In the case of methoxy, the individual rotational lines have not been resolved. However, the experimental lifetimes[10b] are consistent with the lower $\tilde{A}$-state vibrational levels (through v'=6) not being significantly predissociated. Emission has not been observed from the higher vibrational levels, allowing for the possibility that they may be short lived. The spacing of the vibrational levels in methoxy is much smaller than in hydroxy, and the nonradiative stability of the lower levels may simply arise from them being below the energy of the intersecting dissociative states. On the other hand, it may be that the nonradiative mechanism is much weaker in the CH_3O case. To help clarify this situation, we have obtained theoretical estimates of the energies at which the $\check{A}^2A_1$ state intersects the potential surfaces of the ^4E, $^4A_2$, and $^2A_2$ dissociative states.

B. Theoretical method.

Initially, attempts were made to define a limited, valence space CI procedure for location of the surface intersections. However, balanced treatment of the four states was not obtained, and the selected CI method with extrapolation was used instead. Preliminary calculations were carried out in the vicinity of the surface intersections to determine which configurations should be included in the root sets. In the $^2A_1$ case it is known that at dissociation, several root set configurations are needed to correctly describe the

state of the oxygen atom. Since the surface intersections occur at values of R_{CO} that are considerably larger than the equilibrium value, calculations were carried out to assess the importance of the secondary configurations. At the relevant conformations, Conf. (7) accounts for over 90% of the $^2A_1$ CI wave function (based on c^2 criterion), and the most important secondary configurations have coefficient magnitudes of about 0.05 or less. Preliminary calculations on the ^4E, $^4A_2$, and $^2A_2$ states indicated that secondary configurations were even less important in those cases. Therefore, throughout this phase of the study, single space configurations were used for the SCF wave functions and for the CI root sets.

The SCF orbitals for each state were obtained and were transformed into the corresponding ANO's. Cumulative selection with τ in the range $20\text{-}50\times10^{-3}$ h was carried out on master configuration lists containing all single and double excitations. For the dissociative states the principal (root set) configurations are

$$\ldots(3a_1)^2(4a_1)^2(5a_1)^2(6a_1)^1(1e)^4(2e)^2 \qquad {}^4A_2,\ {}^2A_2 \qquad (12)$$

$$\ldots(3a_1)^2(4a_1)^2(5a_1)^1(6a_1)^1(1e)^4(2e)^3 \qquad {}^4E, \qquad (13)$$

in which the $3a_1$ orbital is almost entirely O_{2s}, $4a_1$ and 1e represent the three C-H σ-bonds, the 2e pair are nonbonding O_{2p} orbitals, $5a_1$ is a σ-type orbital mostly (90-95%) on oxygen, and $6a_1$ is a σ^* orbital located mostly on carbon. When considered for the $^2A_1$ state, the main changes are that the $5a_1$ (double occupied) and $6a_1$ (unoccupied) orbitals are more equally delocalized over both carbon and oxygen. To illustrate these differences, the $5a_1$ and $6a_1$ MO's of the ^4E state and the $5a_1$ MO of the $^2A_1$ state are presented in Figs. 4-6 for a conformation near the ^4E - $^2A_1$ intersection.

Near the potential surface intersections the state energies and

their spacings were found to be much more sensitive to small changes in R_{CO} than to changes in the other internal coordinates. Over the range of C-O distances that include all three intersections, the optimum C-H distance for the $^2A_1$ state changes by only 0.01 a_o, affecting the energy by about 0.1 mh. R_{CH} would change by about 0.03 a_o if optimized for the dissociative states, with an energy change of not more than 1.5 mh. The situation is similar when optimization of the HCO bond angle is considered. θ_{HCO} would vary by as much as 2° (.3 mh) for the $^2A_1$ state and 5° (1.3 mh) for the repulsive states if full optimization were allowed. Because the energies are relatively insensitive to small changes in R_{CH} and θ_{HCO}, it was decided to optimize these coordinates at one C-O distance for the $^2A_1$ state and to use the resulting values unchanged for all of the states and conformations being studied. This reduces the apparent complexity of each potential surface intersection from a two dimensional surface to a single point. It is expected that this point will be reasonably close to the lowest point on the full surface of intersection, because further optimization of R_{CH} and θ_{HCO} would lead to relatively small energy changes. With R_{CO} fixed at 1.98 Å, R_{CH} and θ_{HCO} were optimized for the $^2A_1$ state and found to be 1.08 Å and 97°. These values were used in all subsequent calculations.

With R_{CH} and θ_{HCO} fixed at the above values, the energies of the intersecting states were calculated as functions of R_{CO}. These energies, which included CI extrapolation and the Davidson correction for higher excitations, were plotted, and the points of intersection were located graphically. When computing the intersection energy relative to the ^2E ground state, the theoretical results were shifted to accommodate the experimental value of the $\tilde{X}$-$\tilde{A}$ system origin (3.91 eV) since it is thought to be slightly more accurate than the present

theoretical value (3.96 eV).

C. Results and discussion.

The intersection energies of the $^2A_1$ state with each disociative state are given in Table VII. It is seen that the lowest energy intersection is with the $^4A_2$ state and is slightly above the v'=7 vibrational level (Table IV, $^2A_1$, ν_3 normal coord.). The other intersections (with ^4E and $^2A_2$) are close together and, by extrapolation of the data in Table IV, are located between the v'=9 and 10 levels. Assuming an error in the intersection energy of no more than 0.1 eV, the corresponding vibrational quantum numbers are uncertain by no more than unity. These results suggest that the CH_3O radical would not be strongly predissociated in the v'=0-6 levels even if the nonradiative interaction were intrinsically strong. If the interaction is strong, the vibrational levels above v'=7 could be seriously affected, and emission from them might be quenched. In fact, there have been no experimental observations in emission of levels above v'=6. The absorption spectrum of Wendt and Hunziker[4] contains a band identified as v'=8, but it has not been determined if individual rotational lines are broadened in either this or the lower-lying bands.

It is interesting to compare the CH_3O surface intersections with those of the hydroxyl radical. In the OH case, theory and experiment[39,40] indicate that the the weak predissociation[36,37] of the v'=0-2 levels of the $\tilde{A}^2\Sigma^+$ state is due to the intersection of the $\tilde{A}$ state potential curve with the lowest lying dissociative state($^4\Sigma^-$). In the case of methoxy, the $^4A_2$ state is the lowest lying of the dissociative states and its electronic structure is analogous to that of the $^4\Sigma^-$ state of hydroxy. A stronger predissociation occurs[38] in

the hydroxy $\tilde{A}$ state near the v′=5 level. Theory[39] indicates that the $\tilde{A}$ state is crossed by both the $^2\Sigma^-$ and $^4\Pi$ repulsive states in the vicinity of the v′=5 level, with the $^2\Sigma^-$ state being at slightly lower energy. The analogous CH_3O dissociative states, $^2A_2$ and ^4E, are also close together and cross the A state surface between v′=9 and 10. However, in this case, the $^2A_2$ state is predicted to lie slightly above the ^4E state . If the comparison between the OH and CH_3O radicals is valid, it would be reasonable to expect a weak predissociation in the CH_3O $^2A_1$ state near its intersection with the $^4A_2$ state (v′=7), with a stronger effect near the intersections with the $^2A_2$ and ^4E states (v′=9-10).

Simple considerations would lead one to predict that the $^2A_1$ - ^4E nonradiative interaction might be stronger than either the $^2A_1$ -$^4A_2$ or $^2A_1$ - $^2A_2$ ones. Comparison of Conf. (7) with Confs. (12)-(13) shows that the principal $^2A_1$ and ^4E configurations differ formally by one spin orbital ($2e \rightarrow 6a_1$), whereas in both of the other cases the difference is two spin orbitals ($2e^2 \rightarrow 5a_1 6a_1$). The perturbation responsible for the doublet-quartet coupling interactions is the spin orbit operator, a sum of one-electron operators. The dominant contribution to the $^2A_1$ - $^2A_2$ interaction is probably from the off diagonal nuclear kinetic energy operator,

$$\langle \Psi(q;Q) | \partial/\partial Q | \Psi'(q;Q) \rangle (\partial/\partial Q),$$

where Ψ and Ψ' are electronic wave functions for the two states, q represents the electronic coordinates, Q represents the nuclear coordinates, and the integration is over the electronic space. This term can be shown[41] to be equal to

$$\frac{\langle \Psi(q;Q) | \partial \mathcal{H}/\partial Q | \Psi'(q;Q) \rangle (\partial/\partial Q)}{E(Q)-E'(Q)},$$

where E and E′ are the electronic state energies and $\mathcal{U}$ is the electrostatic potential energy operator. The dependence of $\mathcal{U}$ upon Q arises from the electron-nuclear attraction operator and, therefore, $\partial\mathcal{U}/\partial Q$ is a sum of one-electron operators. Thus, to the extent that the principal configurations [(7), (12), and (13)] dominate the full wave functions and that they are based on the same set of molecular orbitals, the rules[42] for evaluating determinantal matrix elements would indicate that these (one-electron) perturbation operators would yield a nonzero coupling only for the $^2A_1$ - ^4E case.

In actuality, of course, the orbitals for the various states are not identical. Note in paticular the difference between the $5a_1$ orbitals in Figs. 4 and 6. Also, there are many important secondary terms in the full wave functions. Although the above discussion cannot be applied rigorously, it does make it plausible that the $^2A_1$ - ^4E interaction would be considerably stronger than the other two. This would result in the strongest predissociation occurring near the $^2A_1$ - ^4E surface intersection. While this has not yet been observed in the methoxy case, the same general argument can also be applied to the OH radical and is consistent with the observations that have been made on that radical.

VI. SUMMARY AND CONCLUSIONS

A. General.

The present study has resulted in a characterization of the $^2A_1$ excited state of CH_3O that is consistent with the usual picture of it as arising through the excitation of an electron from the C-O σ-bonding orbital into a nonbonding oxygen p-orbital. This results in the excited state having a much elongated C-O bond, a relatively shallow potential well, and a large electric dipole moment. Accurate transition energies have been calculated for the $\tilde{A}$-$\tilde{X}$ system and agree very well with spectroscopic data. Harmonic frequencies for the three totally symmetric vibrational modes were calculated and were found to be in reasonable agreement with the available experimental assignments. By modeling the CH_3O radical as a psuedo diatomic, it has been possible to obtain anharmonic vibrational levels for the C-O stretch and to calculate Franck-Condon factors between the $\tilde{A}$ and $\tilde{X}$ states. These factors were found to be in reasonable agreement with the published experimental band intensities.

In general, the present study agrees with and confirms the most recent spectroscopic assignments arising from both the absorption[4] and emission[10b]. Although in the past there has been some uncertainty in assigning the $\tilde{A}$-$\tilde{X}$ system origin, this study confirms that the most recent experimental value of this quantity is correct. It is also predicted that predissociation of the methoxy radical into an oxygen atom and methyl radical would require excitation into the $v'=7$ or 8 level of the A state, corresponding to a minimum photon energy of 4.47 eV (λ=2774 Å). While this has not been confirmed experimentally, it is consistent with the observations. Bands corresponding to the levels

below v'=7 are present in absorption and emission spectra. These bands do not have significantly shortened lifetimes and, based upon these calculations, are not expected to show the effects of predissociation. Bands corresponding to levels with v'=7 and 8 are identified in absorption[4], but it has not been determined if the individual rotational lines are broadened.

B. Importance of methoxy photolysis.

A question addressed by this study was whether or not the photodissociation of methoxy, Eq. (5), is an important enough process to warrant inclusion in atmospheric models. First, considering Eq. (5) as a source of methyl radicals, it must be compared to other methyl sources usually included in the models. Three reactions generally considered to be important in this regard are:

$$CH_4 + OH \rightarrow CH_3 + H_2O \quad (1)$$

$$CH_4 + O(^1D) \rightarrow CH_3 + OH \quad (14)$$

$$CH_4 + Cl \rightarrow CH_3 + HCl \quad (15)$$

Using recommended rate constants[43] and concentration profiles for the various species[1-2], the rates of methyl production due to the three reactions were estimated at several altitudes. Over the altitude range 0-40 km these reactions always provide a rate of methyl production in excess of 10^3 molecules cm^{-3} s^{-1}. At most altitudes, Rxn. (1) is the most important CH_3 source, although Rxn. (15) is of comparable importance at 20 km and Rxn. (14) becomes significant at higher altitudes. The methyl production rates and data used in making these estimates are summarized in Table VIII for Rxn. (1).

To estimate the rate of methoxy photolysis, several approximations have been made. Since we wish to know whether or not it is acceptable

to omit Rxn. (5) from the models, each approximation has been made in such a way so as to maximize the apparent photolysis rate. Thus, any recommendation to omit Rxn. (5) will be conservative in nature.

In choosing a wavelength range for the solar flux, the long wavelength limit is taken to correspond to the minimum energy (4.47 eV) necessary for predissociation as determined in this study. The short wavelength limit is chosen to correspond to the energy of the highest lying vibrational level of the $^2A_1$ state into which excitation will occur. The diminishing magnitude of the Franck-Condon factors, as given in Section IV.B.1, supports the omission of levels above v'=12. By graphical extrapolation of the data in Table IV ($^2A_1$, ν_3 normal mode), the v'=12 level is estimated to be at 7274 cm^{-1}, requiring an excitation energy from the ground state of 4.77 eV. From the available tables of solar flux data[44], we have chosen the wavelength range 2778-2597 Å as closely approximating the desired range of excitation energies, 4.47-4.77 eV.

The absorption cross section[45] σ is taken to be 1.9×10^{-19} cm^2/molecule over the entire wavelength range. This corresponds to the maximum value of the decadic extinction coefficient (50 l $mole^{-1}$ cm^{-1}) found in the absorption spectrum[4]. The predissociation efficiency φ is taken as unity over this wavelength range. These values of σ and φ are obvious over-estimates, but should provide an upper limit for the predissociation rate. The product $J\sigma\varphi$ is an effective first order rate constant for CH_3O predissociation and its calculation is outlined for several altitudes in Table IX. Using model[44] CH_3O number densities, the calculated rates of photolysis are also presented in this table. Comparison of the photolysis rates in Table IX with the chemical rate

estimates in Table VIII shows that predissociation is unimportant as a methyl source throughout the troposphere and stratosphere. Consequently, its effect on the odd oxygen balance of the atmosphere is negligible at all altitudes. Even at the highest altitudes considered, unrealistically high CH_3O concentrations of 10^6 cm^{-3} would be necessary to provide a significant source of methyl radicals.

The solar fluxes listed in Table IX vary strongly with altitude because the wavelength range used falls entirely within the absorption of the ozone layer. If the present calculations had indicated that predissociation could occur at longer wavelengths, the solar flux values used would be much greater. For example, if we were to include all $^2A_1$ methoxy vibrational levels $v'=0-12$ in the predissociation range, the long wavelength limit would become equal to the system origin (3.91 eV or 3171 Å), and the solar flux at all altitudes would be approximately 10^{15} photons cm^{-2} s^{-1}. Throughout the altitude range in Table IX, this flux would still produce a negligible rate of methyl production.

At altitudes less than 10 km, the CH_3O concentration may be considerably larger than the values given in Table IX. If CH_3O is considered to be in a steady state due to Rxns. (3) and (4), its concentration is a function of the rate constants k_3 and k_4 and of the O_2, NO, and CH_3O_2 concentrations. The model study of Logan et al.[2] suggests maximum CH_3O_2 and NO concentrations of $5x10^8$ molecules cm^{-3} and approximately 100 ppt, respectively. Using these concentrations and current values of the rate constants[43], a maximum CH_3O concentration of $1.5x10^3$ molecules cm^{-3} is obtained. Combined with a maximum solar flux of 10^{15} photons cm^{-2} s^{-1}, this yields a photolysis

rate of roughly 0.3 molecules cm^{-3} s^{-1}. There are enough "order of magnitude" numbers in this rate that it would warrant further consideration if the flux could realistically be that large. However, the present calculations are accurate enough to make us confident that such low lying vibrational levels are not predissociated.

Other photodissociation processes, such as direct excitation from the ground state of methoxy into its repulsive states or dissociation to the $O(^1D)$ asymptote, have not been considered here. However, the semiquantitative potential curves of Fig. 1 suggest that the $\tilde{A}$ - $\tilde{X}$ vertical excitation is the only one at reasonably low energies. Direct dissociation to $O(^1D)$, requires an excitation wavelength less than 2130 A and could not be important below 40 km.

One additional possibility is that the $\tilde{A} \leftarrow \tilde{X}$ excitation of methoxy would be followed by interconversion to upper vibrational levels of the ground state, with subsequent dissociation. The thermodynamic CH_3—O dissociation energy[46] (89 kcal/mole) and the calculated[19] barrier for H—CH_2O dissociation (34 kcal/mole) are both less than the energy of the $\tilde{A}$ - $\tilde{X}$ system origin (3.91 eV, 90.2 kcal/mole). However, this interconversion is not expected to be fast because of the large $^2A_1$ - ^2E "energy gap", a situation that is similar to the generally slow S1 → S0 interconversion of singlet states. Furthermore, as noted previously, the lifetimes of the $^2A_1$ levels with v' less than 7 have been measured and do not show evidence of this dissociation[10b].

Rxn. (5) also serves as a sink for the CH_3O radical. However, the dominant sink is hydrogen abstraction by O_2 to form formaldehyde, Rxn. (4). Due to the abundance of O_2, the rate of this reaction is so great that photolysis is completely negligible as a CH_3O sink (by at least

six orders of magnitude).

ACKNOWLEDGMENTS

The author wishes to thank Dr. Robert E. Boughner of NASA Langley Research Center for making available atmospheric modeling results and Dr. D. H. Phillips, also of NASA Langley Research Center, for several helpful scientific discussions. He also wishes to thank Mr. John Williams of Wake Forest University for implementing the molecular orbital plotting program and generating the contour plots. This material is based upon work supported by the National Aeronautics and Space Administration under Cooperative Agreement NCC1-55 and by the National Science Foundation under Grant PRM 8121880.

REFERENCES

1. a) J. A. Logan, M. J. Prather, S. C. Wofsy and M. B. McElroy, Philos. Trans. R. Soc. London Ser. A 290, 187 (1978); b) B. A. Thrush, Philos. Trans. R. Soc. London Ser. A 296, 149 (1980); c) J. Heicklen, Atmospheric Chemistry (Academic Press, New York, 1976).
2. a) J. A. Logan, M. J. Prather, S. C. Wofsy and M. B. McElroy, J. Geophys. Res. 86C, 7210 (1981); b) H. Levy, II, Planet. Space Sci. 21, 575 (1973); c)"Chemical Kinetic Data Needs for Modeling the Lower Troposphere", edited by J. T. Herron, R. E. Huie and J. A. Hodgeson, NBS Special Publication 557 (August, 1979).
3. C. F. Jackels, J. Chem. Phys. 76, 505 (1982).
4. H. R. Wendt and H. E. Hunziker, J. Chem. Phys. 71, 5202 (1979).
5. a) K. Ohbayashi, H. Akimoto and I. Tanaka, J. Phys. Chem. 81, 798 (1977); b) T. Ebata, H. Yanagishita, K. Obi and I. Tanaka, Chem. Phys. 69, 27 (1982).
6. M. Sutoh, N. Washida, H. Akimoto, M. Nakamura and M. Okuda, J. Chem. Phys. 73, 591 (1980).
7. D. W. G. Style and J. C. Ward, Trans. Faraday Soc. 49, 999 (1953).
8. N. Sanders, J. E. Butler, L. R. Pasternack and J. R. McDonald, Chem. Phys. 48, 203 (1980).
9. D. E. Powers, J. B. Hopkins and R. E. Smalley, J. Phys. Chem. 85, 2711 (1981).
10. a) G. Inoue, H. Akimoto and M. Okuda, Chem. Phys. Lett. 63, 213 (1979); b) J. Chem. Phys. 72, 1769 (1980).
11. a) H. E. Radford and D. K. Russell, J. Chem. Phys. 66, 2222 (1977); b) D. K. Russell and H. E. Radford, J. Chem. Phys. 72, 2750 (1980).
12. M. Iwasaki and K. Toriyama, J. Am. Chem. Soc. 100, 1964 (1978).

13. P. C. Engelking. G. B. Ellison and W. C. Lineberger, J. Chem. Phys. 69, 1826 (1978).

14. a) K. J. Reed and J. I. Brauman, J. Am. Chem. Soc. 97, 1625 (1975); b) B. K. Janousek, A. H. Zimmerman, K. J. Reed and J. I Brauman, J. Am. Chem. Soc. 100, 6142 (1978).

15. D. R. Yarkony, H. F. Schaefer III and S. Rothenberg, J. Am. Chem. Soc. 96, 656 (1974).

16. M-H. Whangbo, S. Wolfe and F. Bernardi, Can. J. Chem. 53, 3040 (1975).

17. a) G. F. Adams, G. D. Bent, G. D. Purvis and R. J. Bartlett, Chem. Phys. Lett. 81, 461 (1981); b) G. F. Adams, R. J. Bartlett and G. D. Purvis, Chem. Phys. Lett. 87, 311 (1982); c) G. D. Bent, G. F. Adams, R. H. Bartram, G. D. Purvis and R. J. Bartlett, J. Chem. Phys. 76, 4144 (1982).

18. R. A. Bair and W. A. Goddard III, J. Am. Chem. Soc. 104, 2719 (1982).

19. S. Saebo, L. Radom and H. F. Schaefer III, J. Chem. Phys. 78, 845 (1983).

20. D. L. Cooper, J. Chem. Phys. 76, 2765 (1982).

21. T. H. Dunning Jr., J. Chem. Phys. 53, 2823 (1970).

22. S. Huzinaga, J. Chem. Phys. 42, 1293 (1965).

23. The integrals were computed with the MOLECULE program, written by J. Almlof. The SCF and CI programs used were the NASA Langley codes, largely adapted and developed by C. W. Bauschlicher.

24. Z. Gershgorn and I. Shavitt, Int. J. Quantum Chem. 2, 751 (1968); M. J. M. Bernal and S. F. Boys, Philos. Trans. R. Soc. London Ser. A 245, 139 (1952).

25. R. C. Raffenetti, K. Hsu and I. Shavitt, Theor. Chim. Acta 45, 33 (1977).

26. Strictly speaking, this refers to the approximate first-order wave function as defined in: H. F. Schaefer III, J. Chem. Phys. 54, 2207 (1971).

27. T. L. Barr and E. R. Davidson, Phys. Rev. A 1, 644 (1970).

28. P. -O. Lowdin, Phys. Rev. 97, 1474 (1955).

29. a) G. T. Surratt and W. A. Goddard III, Chem. Phys. 23, 39 (1977); b) Y. Ishikawa and R. C. Binning Jr., Chem. Phys. Lett. 40, 342 (1976).

30. a) P. Hennig, W. P. Kraemer, G. H. F. Diercksen and G. Strey, Theor. Chim. Acta 47, 233 (1978); b) R. J. Whitehead and N. C. Handy, J. Mol. Spectrosc. 59, 459 (1976); c) B. J. Rosenberg, W. C. Ermler and I. Shavitt, J. Chem. Phys. 65, 4072 (1976).

31. E. B. Wilson, Jr., J. C. Decius and P. C. Cross, Molecular Vibrations (McGraw-Hill, New York, 1955), Chap. 4.

32. D. F. McIntosh and K. H. Michaelian, Can. J. Spectrosc. 24, 1 (1979); Can. J. Spectrosc. 24, 35 (1979); Can. J. Spectrosc. 24, 65 (1979).

33. F. L. Tobin and J. Hinze, J. Chem. Phys. 63, 1034 (1975).

34. C. F. Jackels and I. Shavitt, Theor. Chim. Acta 58, 81 (1981); R. J. Buenker and S. D. Peyerimhoff, Theor. Chim. Acta 39, 217 (1975).

35. E. R. Davidson in The World of Quantum Chemistry, edited by R. Daudel and B. Pullman (Reidel, Dordrecht-Holland, 1974).

36. A. G. Gaydon and H. G. Wolfhard, Proc. R. Soc. London, Ser A 208, 63 (1951).

37. R. A. Sutherland and R. A. Anderson, J. Chem. Phys. 58, 1226 (1973).

38. C. Carlone and F. W. Dalby, Can. J. Phys. 47, 1945 (1969).

39. H. H. Michels and F. E. Harris, Chem. Phys. Lett. 3, 441 (1969).

40. H. B. Palmer and D. W. Naegeli, J. Mol. Spectrosc. 28, 417 (1968).

41. P. Avouris, W. M. Gelbart and M. A. El-Sayed, Chem. Rev. 77, 793 (1977).

42. E. U. Condon and G. H. Shortley, The Theory of Atomic Spectra (Cambridge University, London, 1967), chapter 6.

43. NASA, "Chemical Kinetics and Photochemical Data for Use in Stratospheric Modeling, Evaluation Number 6", NASA Panel for Data Evaluation, Publ. 83-62, (Jet Propulsion Laboratory, Pasadena, California, 1983).

44. NASA Langley one-dimensional scattering model for atmospheric photochemistry,

details to be published by R. E. Boughner; see also L. B. Callis, Paper 72663,in Proceedings of the 5th Fluid and Plasma Dynamics Conference (Boston, 1974),(American Institute of Aeronautics and Astronautics, New York, 1974).

45. Defined by the Beer's Law expression $I = I_o \exp(-\sigma n l)$, where σ is the absorption cross section in cm^2/molecule, n is the concentration in molecule/cm^3, and l is the pathlength in cm.

46. Calculated from heat of formation data, in Handbook of Physics and Chemistry, edited by Robert C. Weast (Chemical Rubber, Cleveland, 1981), 62nd edition.

TABLE I. Theoretical Values of the Ground and Excited State Equilibrium Geometries of the Methoxy Radical.

Method	R_{CO}^e(Å)	R_{CH}^e(Å)	Θ_{HCO}^e(deg)	Ref.
^2E State				
First-Order CI	1.413(4)	1.112(4)	109.0(5)	this study[a]
MBPT	1.41	...	...	17c
GVB-CI	1.410	1.111,1.112	106.9,111.1	18
UHF	1.386	1.087	109.9	19
$^2A_1$ State				
First-Order CI	1.614(6)	1.091(2)	102.6(2)	this study[a]
SCF	1.65	1.08	102	15

a. Numbers in parenthesis are uncertainties in the last figure due to precision limitations of the potential surface analytical fit and of the search for its minimum. These values do not reflect the inherent accuracy limitations of the present CI method.

TABLE II. Quadratic Force Constants for the Methoxy Radical.

Force Constant[a]	$\tilde{X}^2E$ State[b]	$\tilde{A}^2A_1$ State[b]
k_{200}	0.163	0.968×10^{-1}
k_{110}	0.454×10^{-1}	0.715×10^{-1}
k_{020}	0.527	0.597
k_{101}	0.278×10^{-2}	0.333×10^{-2}
k_{011}	0.226×10^{-3}	-0.671×10^{-3}
k_{002}	0.122×10^{-3}	0.115×10^{-3}

a. The symbols k_{ijk} are defined in Eq(9) of the text.

b. The constants k_{200}, k_{110}, and k_{020} are in hartree/bohr^2; k_{101} and k_{011} are in hartree/bohr-deg; and k_{002} is in hartree/deg^2.

TABLE III. Vibrational Energies (in cm^{-1}) for the CH_3O and CD_3O Radicals.

Vibrational Mode	CH_3O			CD_3O	
	This work[a]	HF/631-G[b]	Exptl	This work[a]	Exptl
^2E State					
ν_1	3071	3188	...	2203	...
ν_2	1335	1585	1325[c]	955	1010[c]
ν_3	1048	1130	1022[d]	1071	1005[d]
$^2A_1$ State					
ν_1	3239	...	...	2298	...
ν_2	1308	...	...	968	...
ν_3	733	...	676[e]	732	644[d]

a. calc harm frequencies.

b. Ref. 19

c. Ref. 13

d. Ref. 10b

e. Ref. 4

TABLE IV. Calculated Vibrational Energy Levels of Methoxy as a Pseudo Diatomic Molecule.

State	Vibrational Coordinate	Energies[a] (cm^{-1})
^2E	C-O distance[b]	544, 1623, 2685, 3729, 4753, 5755, 6733, 7682, 8598, 9472, ...
	ν_3 normal mode[c]	536, 1600, 2648, 3678, 4688, 5676, 6640, 7577, 8481, 9249, ...
$^2A_1$	C-O distance[b]	375, 1119, 1853, 2575, 3285, 3981, 4661, 5326, 5973, 6602, ...
	ν_3 normal mode[c]	352, 1048, 1729, 2393, 3038, 3660, 4256, 4821, 5361, 5884, ...

a. Relative to the minimum of the potential curve.

b. Distance from oxygen atom to the center of mass of methyl moiety.

c. As determined from three-dimensional harmonic analysis.

TABLE V. Calculated Energies (in hartrees).

State	SCF	CI(τ=15mh)	CI($\tau\rightarrow$0)	ΔE_q
$\tilde{X}$ state eq. conformation				
^2E	-114.44560	-114.72775	-114.73849	-0.02476
$^2A_1$	-114.29285	-114.57127	-114.58231	-0.02386
$\tilde{A}$ state eq. conformation				
^2E	-114.42331	-114.70766	-114.71852	-0.02625
$^2A_1$	-114.30483	-114.58179	-114.59280	-0.02445

TABLE VI. Transition Energies (in eV) for the $\tilde{A}^2A_1$ - $\tilde{X}^2E$ System of the Methoxy Radical.

Level of Theory	Vert. Excitation[a] $^2A_1 \leftarrow {}^2E$	Vert. Deexcitation[b] $^2A_1 \rightarrow {}^2E$	System Origin[c] (0,0) band
SCF	4.16	3.22	3.83
CI(τ=15mh)	4.26	3.42	3.97
Extrap. CI	4.25	3.42	3.96
Extrap. CI + ΔE_q	4.27	3.47	3.97
Extrap. CI + ΔE_q + vib corr	4.21	3.52	3.96

a. Both state energies calculated at ^2E eq. conformation.

b. Both state energies calculated at $^2A_1$ eq. conformation.

c. Each state energy calculated at its own eq. conformation.

TABLE VII. Energies of Intersection Between the $\tilde{A}^2A_1$ and Repulsive States of the Methoxy Radical.

Intersection	C-O distance at intersection (A)	Energy relative to $^2A_1$ minimum (cm^{-1})	Energy relative to ground state (eV)
$^2A_1$-$^4A_2$	2.01	4883	4.47
$^2A_1$-^4E	2.07	6222	4.64
$^2A_1$-$^2A_2$	2.09	6398	4.66

TABLE VIII. Rate of methyl production due to reaction of the hydroxyl radical with methane.

Altitude (km)	T[a] (K)	rate const.[b] k (cm^3/molecule s)	$[CH_4]$[c] (molecule/cm^3)	[OH][d] (molecule/cm^3)	rate[e] (molecule/cm^3 s)
0	291	6.7×10^{-15}	3.5×10^{13}	10^6	2.3×10^5
20	219	9.8×10^{-16}	1.7×10^{12}	10^6	1.7×10^3
40	268	4.1×10^{-15}	2.4×10^{10}	3×10^7	3.0×10^3

a. Ref. 1c

b. $k=2.4 \times 10^{-12} \exp(-1710/T)$ for $OH + CH_4 \rightarrow CH_3 + H_2O$, Ref. 43.

c. derived from Fig. 8, Ref. 1a

d. Fig 27, Ref. 2a and Fig 14a, Ref. 1a

e. rate=$k[CH_4][OH]$

TABLE IX. Calculated photolysis rate of the methoxy radical.

Altitude (km)	Solar Flux J^a (photons/cm^2 s)	Photol. Const. $k_{phot}{}^b$ (s^{-1})	$[CH_3O]^c$ (molecule/cm^3)	rate^d (molecule/cm^3 s)
10	1.5×10^{-8}	2.8×10^{-27}	28	8.0×10^{-26}
16	6.6×10^{-7}	1.3×10^{-25}	7.6	9.9×10^{-25}
22	6.4×10^{-1}	1.2×10^{-19}	117	2.1×10^{-18}
28	2.7×10^{7}	5.1×10^{-12}	62	3.2×10^{-10}
34	5.6×10^{11}	1.1×10^{-7}	135	1.5×10^{-5}
40	5.7×10^{13}	1.1×10^{-5}	162	1.8×10^{-3}
46	2.7×10^{14}	5.1×10^{-5}	121	6.2×10^{-3}

a. From NASA model (Ref. 44), integrated over range λ = 277.8-259.7 nm.

b. Calculated as equal to $J\sigma\varphi$, with $\sigma=1.9\times10^{-19}$cm^2/molecule and φ=1 molecule/photon.

c. NASA model (Ref. 44), diurnal average, and at photochemical equilibrium.

d. rate=k_{phot} $[CH_3O]$.

FIGURE CAPTIONS

Fig. 1. Potential energy curves of the methoxy radical at C_{3v} conformations. R_{CH} = 2.041 a_o; θ_{HCO} decreases from 113 to 90° as R_{CO} increases from 2.27 to 5.67 a_o. (Reproduced from Ref. 3)

Fig. 2. $^2A_1$ Potential energy curves of the methoxy radical as functions of the C-O distance and ν_3 normal coordinate. ΔR_{CO} is obtained in bohrs by multiplying the abscissa value by 0.378 (dashed curve) or 0.359 (solid curve). Energy levels are for the dashed curve.

Fig. 3. The $5a_1$ SCF molecular orbital for the CH_3O $^2A_1$ state, in an HCO plane, at the $^2A_1$ equilibrium conformation: R_{CO}= 1.61 Å, R_{CH}= 1.09 Å, and θ_{HCO}= 102.6°. Contours enclose 90, 70, 50, 30, and 10% of integrated three dimensional probability. Major tic spacing = 2 a_o.

Fig. 4. The $5a_1$ SCF molecular orbital for the CH_3O ^4E state, in an HCO plane, at the conformation: R_{CO} = 2.08 Å, R_{CH} = 1.08 Å, and θ_{HCO}= 97.0°. Contours and tic spacing as in Fig. 3.

Fig. 5. The $6a_1$ SCF molecular orbital for the CH_3O ^4E state. Conformation, contours, and tic spacing as in Fig. 4.

Fig. 6. The $5a_1$ SCF molecular orbital for the CH_3O $^2A_1$ state. Conformation, contours, and tic spacing as in Fig. 4.

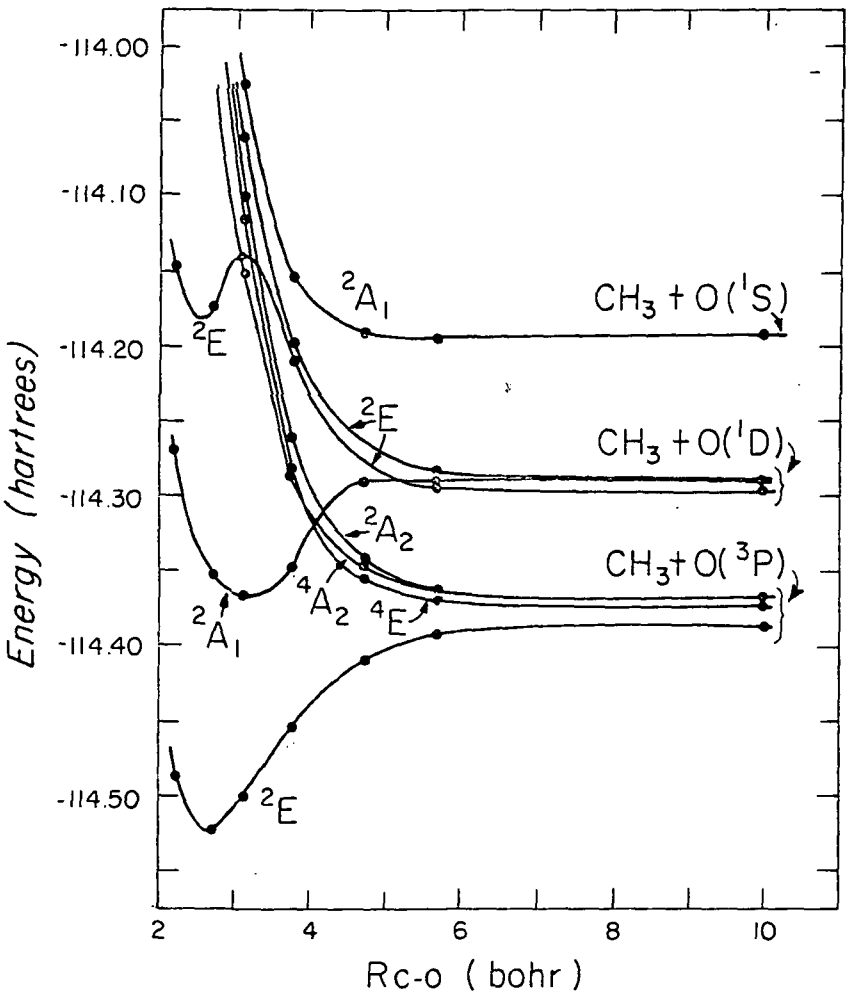
-114.00
-114.10
-114.20
-114.30
-114.40
-114.50
Energy (hartrees)
2
4
6
8
10
Rc-o (bohr)
$^2A_1$
^2E
$CH_3 + O(^1S)$
^2E
$CH_3 + O(^1D)$
$^2A_2$
$CH_3 + O(^3P)$
$^4A_2$
^4E
$^2A_1$
^2E

Figure 1

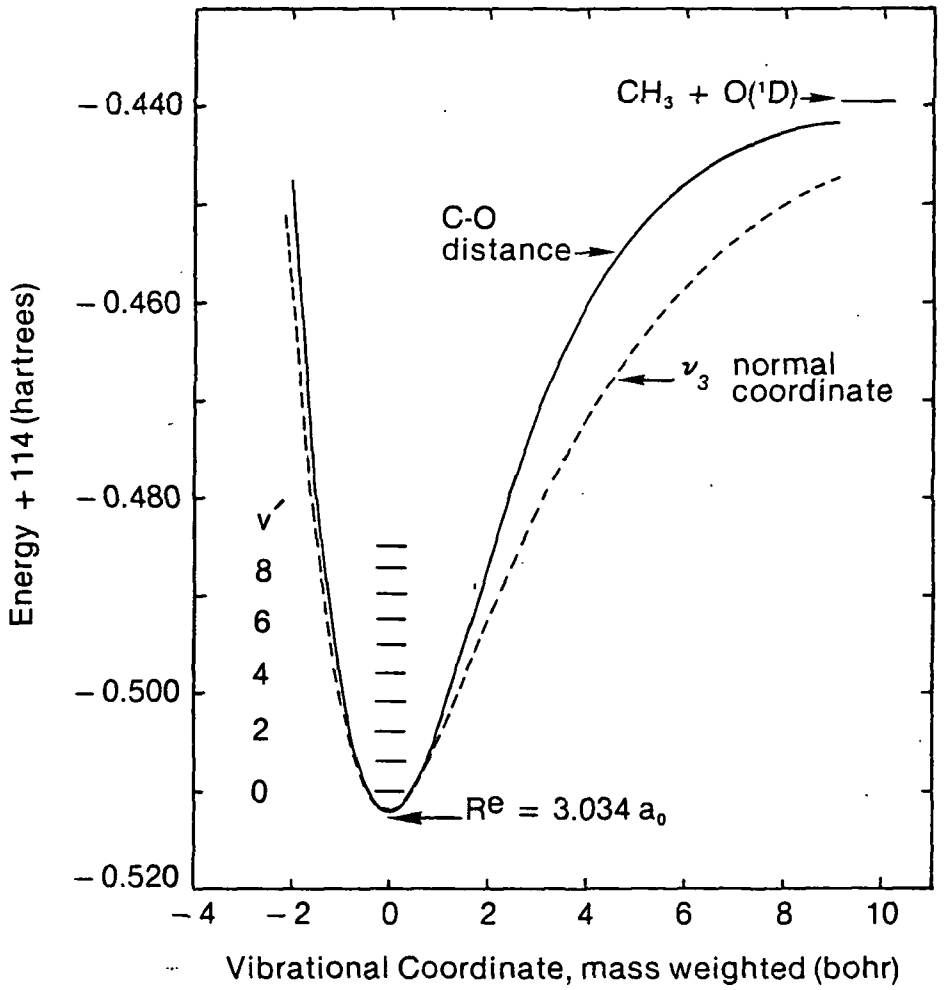
Energy + 114 (hartrees)
−0.440
−0.460
−0.480
−0.500
−0.520
CH₃ + O(¹D)
C-O distance
ν₃ normal coordinate
v'
8
6
4
2
0
Re = 3.034 a₀
−4
−2
0
2
4
6
8
10
Vibrational Coordinate, mass weighted (bohr)

Figure 2

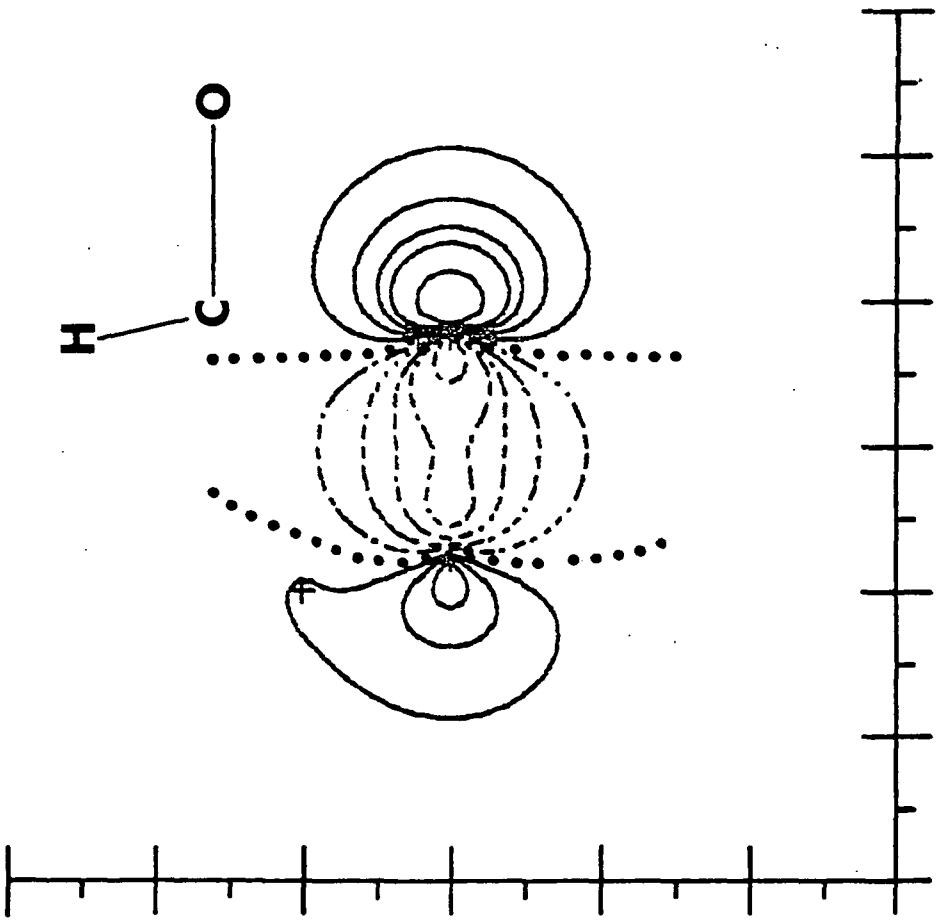

Figure 3

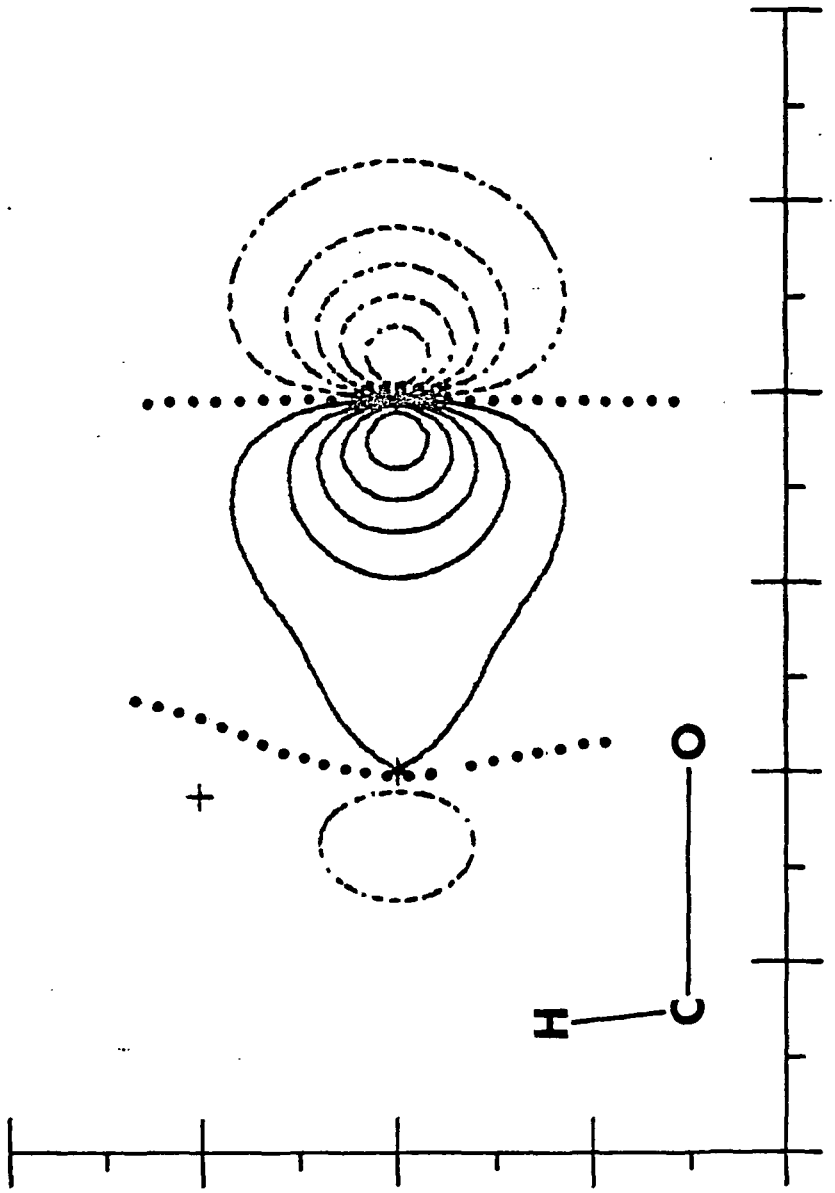

Figure 4

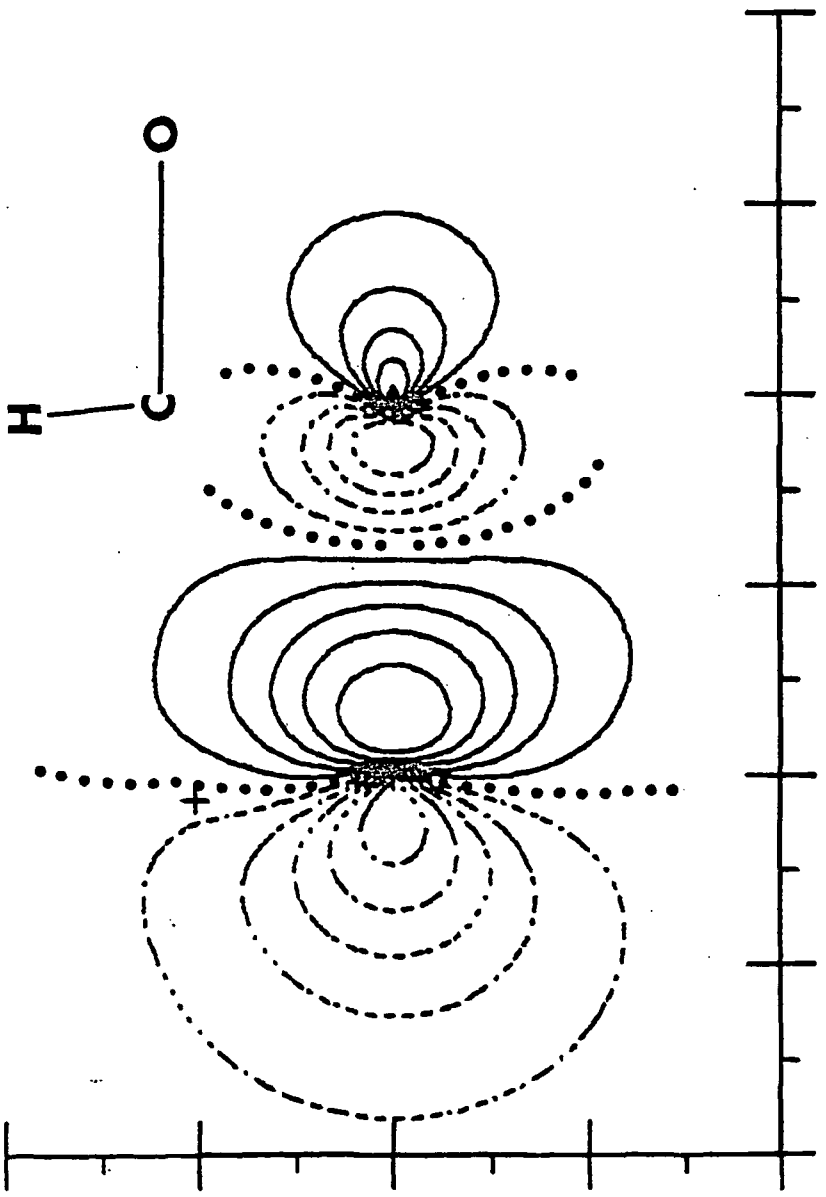

Figure 5

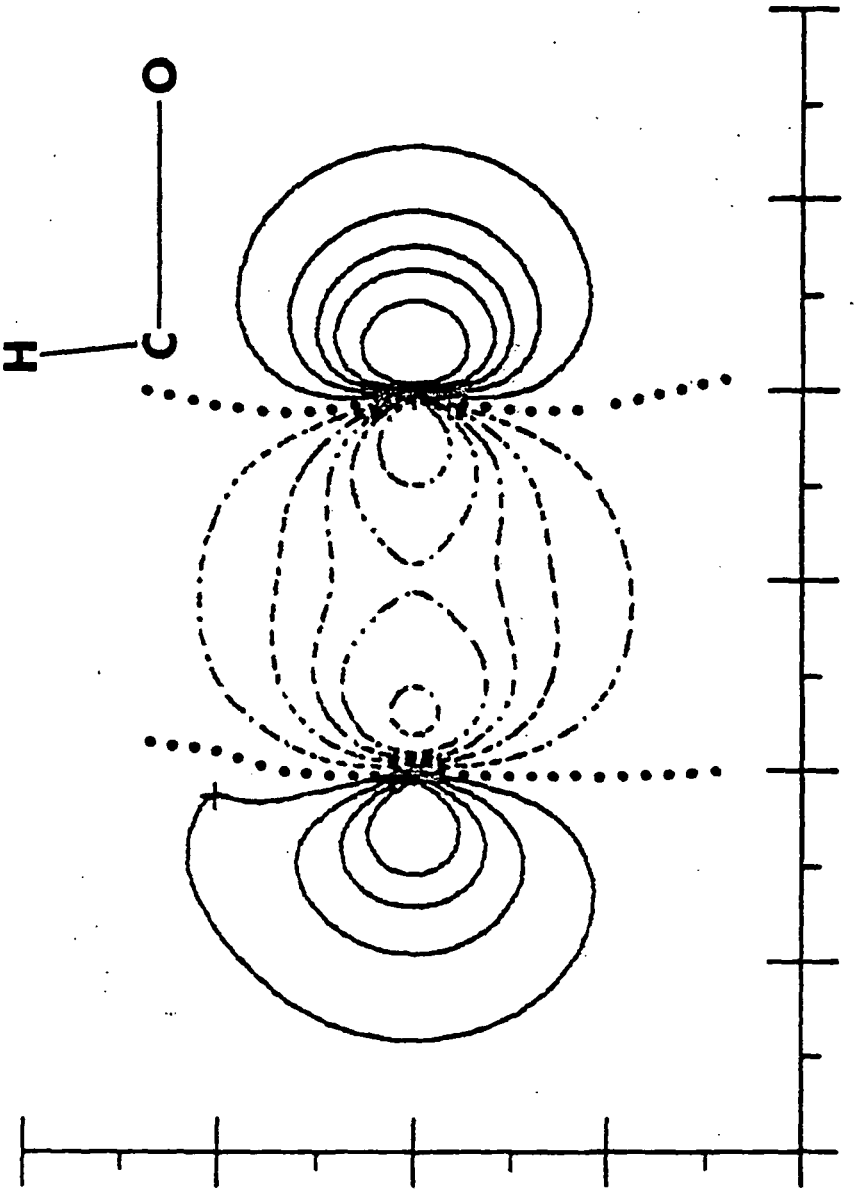

Figure 6